Biomedical Optics EXPRESS

Phthalocyanine photosensitizers as contrast agents for *in vivo* photoacoustic tumor imaging

Amalina Bte Ebrahim Attia,[1] Ghayathri Balasundaram,[1] Wouter Driessen,[2,3] Vasilis Ntziachristos,[2,4] and Malini Olivo[1,5,*]

[1]*Bio-Optical Imaging Group, Singapore Bioimaging Consortium, Helios #01-02, 11 Biopolis Way, Singapore*
[2]*Institute for Biological and Medical Imaging, Helmholtz Zentrum Munich, Technical University Munich, Munich, Germany*
[3]*iThera Medical, GmbH, Germany*
[4]*Technical University of Munich, Germany*
[5]*School of Physics, National University of Ireland, Galway, Ireland*
[*] *malini_olivo@sbic.a-star.edu.sg*

Abstract: There is a need for contrast agents for non-invasive diagnostic imaging of tumors. Herein, Multispectral Optoacoustic Tomography (MSOT) was employed to evaluate phthalocyanines commonly used in photodynamic therapy as photoacoustic contrast agents. We studied the photoacoustic activity of three water-soluble phthalocyanine photosensitizers: phthalocyanine tetrasulfonic acid (PcS4), Zn(II) phthalocyanine tetrasulfonic acid (ZnPcS4) and Al(III) phthalocyanine chloride tetrasulfonic acid (AlPcS4) in phantom and in tumor-bearing mice to investigate the biodistribution and fate of the phthalocyanines in the biological tissues. PcS4 was observed to grant good contrast between the different reticuloendothelial organs and accumulate in the tumor within an hour of post-administration. ZnPcS4 and AlPcS4 offered little contrast in photoacoustic signals between the organs. PcS4 is a promising photoacoustic contrast agent and can be exploited as a photodiagnostic agent.

OCIS codes: (110.5125) Photoacoustics; (170.5120) Photoacoustic imaging; (110.4234) Multispectral and hyperspectral imaging; (160.1050) Acousto-optical materials; (170.6930) Tissue; (170.3880) Medical and biological imaging

References and links

1. A. Hellebust and R. Richards-Kortum, "Advances in molecular imaging: targeted optical contrast agents for cancer diagnostics," Nanomedicine (Lond) **7**(3), 429–445 (2012).
2. V. Ntziachristos, C. Bremer, and R. Weissleder, "Fluorescence imaging with near-infrared light: new technological advances that enable *in vivo* molecular imaging," Eur. Radiol. **13**(1), 195–208 (2003).
3. J. G. Fujimoto, C. Pitris, S. A. Boppart, and M. E. Brezinski, "Optical coherence tomography: an emerging technology for biomedical imaging and optical biopsy," Neoplasia **2**(1-2), 9–25 (2000).
4. L. V. Wang, "Multiscale photoacoustic microscopy and computed tomography," Nat. Photonics **3**(9), 503–509 (2009).
5. L. V. Wang and S. Hu, "Photoacoustic tomography: *in vivo* imaging from organelles to organs," Science **335**(6075), 1458–1462 (2012).
6. R. O. Esenaliev, A. A. Karabutov, and A. A. Oraevsky, "Sensitivity of laser opto-acoustic imaging in detection of small deeply embedded tumors," IEEE J. Sel. Top. Quantum Electron. **5**(4), 981–988 (1999).
7. G. Ku and L. V. Wang, "Deeply penetrating photoacoustic tomography in biological tissues enhanced with an optical contrast agent," Opt. Lett. **30**(5), 507–509 (2005).
8. T. L. Troy, D. L. Page, and E. M. Sevick-Muraca, "Optical properties of normal and diseased breast tissues: prognosis for optical mammography," J. Biomed. Opt. **1**(3), 342–355 (1996).
9. G. P. Luke, D. Yeager, and S. Y. Emelianov, "Biomedical applications of photoacoustic imaging with exogenous contrast agents," Ann. Biomed. Eng. **40**(2), 422–437 (2012).
10. L. Nie and X. Chen, "Structural and functional photoacoustic molecular tomography aided by emerging contrast agents," Chem. Soc. Rev. **43**(20), 7132–7170 (2014).
11. W. S. Poon, K. T. Schomacker, T. F. Deutsch, and R. L. Martuza, "Laser-induced fluorescence: experimental intraoperative delineation of tumor resection margins," J. Neurosurg. **76**(4), 679–686 (1992).

#224155 - $15.00 USD Received 30 Sep 2014; revised 3 Dec 2014; accepted 3 Dec 2014; published 26 Jan 2015

12. M. J. Witjes, O. C. Speelman, P. G. Nikkels, C. A. Nooren, J. M. Nauta, B. van der Holt, H. L. van Leengoed, W. M. Star, and J. L. Roodenburg, "In vivo fluorescence kinetics and localisation of aluminum phthalocyanine disulphonate in an autologous tumour model," Br. J. Cancer **73**(5), 573–580 (1996).
13. G. A. Wagnières, W. M. Star, and B. C. Wilson, "In vivo fluorescence spectroscopy and imaging for oncological applications," Photochem. Photobiol. **68**(5), 603–632 (1998).
14. C. J. H. Ho, G. Balasundaram, W. Driessen, R. McLaren, C. L. Wong, U. S. Dinish, A. B. E. Attia, V. Ntziachristos, and M. Olivo, "Multifunctional Photosensitizer-Based Contrast Agents for Photoacoustic Imaging," Sci. Rep. **4**, 5342 (2014).
15. N. Sekkat, H. van den Bergh, T. Nyokong, and N. Lange, "Like a bolt from the blue: phthalocyanines in biomedical optics," Molecules **17**(1), 98–144 (2012).
16. A. Beeby, S. FitzGerald, and C. F. Stanley, "A photophysical study of protonated (tetra-tert-butylphthalocyaninato) zinc," J. Chem. Soc., Perkin Trans. 2 **2001**(10), 1978–1982 (2001).
17. H. L. van Leengoed, V. Cuomo, A. A. Versteeg, N. van der Veen, G. Jori, and W. M. Star, "*In vivo* fluorescence and photodynamic activity of zinc phthalocyanine administered in liposomes," Br. J. Cancer **69**(5), 840–845 (1994).
18. A. Beeby, S. FitzGerald, and C. F. Stanley, "Protonation of Tetrasulfonated Zinc Phthalocyanine in Aqueous Acetonitrile Solution," Photochem. Photobiol. **74**(4), 566–569 (2001).
19. N. B. R. Vittar, C. G. Prucca, C. Strassert, J. Awruch, and V. A. Rivarola, "Cellular inactivation and antitumor efficacy of a new zinc phthalocyanine with potential use in photodynamic therapy," Int. J. Biochem. Cell Biol. **40**(10), 2192–2205 (2008).
20. B. Zhao, J.-J. Yin, P. J. Bilski, C. F. Chignell, J. E. Roberts, and Y.-Y. He, "Enhanced photodynamic efficacy towards melanoma cells by encapsulation of Pc4 in silica nanoparticles," Toxicol. Appl. Pharmacol. **241**(2), 163–172 (2009).
21. R. Ma, A. Taruttis, V. Ntziachristos, and D. Razansky, "Multispectral optoacoustic tomography (MSOT) scanner for whole-body small animal imaging," Opt. Express **17**(24), 21414–21426 (2009).
22. V. Ntziachristos and D. Razansky, "Molecular imaging by means of multispectral optoacoustic tomography (MSOT)," Chem. Rev. **110**(5), 2783–2794 (2010).
23. A. Rosenthal, D. Razansky, and V. Ntziachristos, "Fast semi-analytical model-based acoustic inversion for quantitative optoacoustic tomography," IEEE Trans. Med. Imaging **29**(6), 1275–1285 (2010).
24. S. Tzoumas, N. Deliolanis, S. Morscher, and V. Ntziachristos, "Un-mixing Molecular Agents from Absorbing Tissue in Multispectral Optoacoustic Tomography," IEEE Trans. Med. Imaging **33**(1), 48–60 (2014).
25. D. Razansky, C. Vinegoni, and V. Ntziachristos, "Multispectral photoacoustic imaging of fluorochromes in small animals," Opt. Lett. **32**(19), 2891–2893 (2007).
26. Z. Li, H. Li, Z. Zeng, W. Xie, and W. R. Chen, "Determination of optical absorption coefficient with focusing photoacoustic imaging," J. Biomed. Opt. **17**(6), 061216 (2012).
27. J. Liu, J. Geng, L.-D. Liao, N. Thakor, X. Gao, and B. Liu, "Conjugated polymer nanoparticles for photoacoustic vascular imaging," Polym. Chem. **5**(8), 2854–2862 (2014).
28. A. Abuteen, S. Zanganeh, J. Akhigbe, L. P. Samankumara, A. Aguirre, N. Biswal, M. Braune, A. Vollertsen, B. Röder, C. Brückner, and Q. Zhu, "The evaluation of NIR-absorbing porphyrin derivatives as contrast agents in photoacoustic imaging," Phys. Chem. Chem. Phys. **15**(42), 18502–18509 (2013).
29. A. Ogunsipe and T. Nyokong, "Photophysical and photochemical studies of sulphonated non-transition metal phthalocyanines in aqueous and non-aqueous media," J. Photochem. Photobiol. Chem. **173**(2), 211–220 (2005).
30. A. Borgatti-Jeffreys, S. B. Hooser, M. A. Miller, and M. D. Lucroy, "Phase I clinical trial of the use of zinc phthalocyanine tetrasulfonate as a photosensitizer for photodynamic therapy in dogs," Am. J. Vet. Res. **68**(4), 399–404 (2007).
31. University of Arkansas for Medical Sciences, Department of Neurobiology and Developmental Sciences, "Arteries of the Abdomen- Arranged Alphabetically," http://anatomy.uams.edu/arteries_abdomen.html.
32. University of Arkansas for Medical Sciences, Department of Neurobiology and Developmental Sciences, "Selected Veins of the Abdomen - Listed Alphabetically," http://anatomy.uams.edu/veins_abdomen.html.
33. H. L. van Leengoed, N. van der Veen, A. A. Versteeg, R. Ouellet, J. E. van Lier, and W. M. Star, "*In vivo* fluorescence kinetics of phthalocyanines in a skin-fold observation chamber model: role of central metal ion and degree of sulfonation," Photochem. Photobiol. **58**(2), 233–237 (1993).

1. Introduction

With more than 10 million cancer malignancies in the oral cavity, oropharynx and esophagus diagnosed each year, there arises a need for reliable contrast agents for early and easy detection [1]. Optical imaging has undisputedly been widely used as an imaging modality in such diagnostic imaging by virtue of their portability, low cost and ability to give real-time macroscopic images of organs. Most commonly employed optical contrast agents are fluorophores that absorb or emit in the near-infrared (NIR) region whereby there exists low light absorption and scattering, and low autofluorescence in the tissues [2]. However, the use

#224155 - $15.00 USD Received 30 Sep 2014; revised 3 Dec 2014; accepted 3 Dec 2014; published 26 Jan 2015

of fluorescent optical imaging systems is limited by their small penetration depth (up to 2-3 mm [3]).

Photoacoustic (PA) imaging has recently gained interest due to its use of non-radioactive probes, low expense and ease of use [4, 5]. PA imaging involves radiating the biological tissue with short, NIR light pulses which are absorbed by the endogenous (e.g. hemoglobin and melanin) or exogenous contrast agents with characteristic absorption spectra in the NIR range, thereby producing heat. The heat causes thermoelastic expansion of the tissue, generating non-scattering acoustic waves to be detected by ultrasound transducers. PA signal generation is governed by the absorption of light by the contrast agents and not by their emitted fluorescence. The higher penetration depth conferred by PA imaging (5-6 cm) [6, 7] while maintaining high spatial resolution and image contrast additionally makes it a desirable imaging modality.

Notably, many types of cancers in their early stages cannot be distinguished by their endogenous vascular contrast [8]. The introduction of exogenous contrast agents in the biological tissues can help improve imaging contrast while giving functional anatomical, cellular and molecular information [9, 10]. However, it proves arduous to select appropriate exogenous PA contrast agents from the immense number available, bearing in mind factors such as biocompatibility, efficiency of PA signal generation, solubility and stability. Photosensitizers have been reported as fluorescent contrast agents to delineate tumor margins in fluorescence endoscopy due to their strong fluorescence and tumor-localizing attributes [11–13]. Herein, we propose the use of photosensitizer-based contrast agents as photoacoustic contrast agents for deep tissue and tomographic imaging *via* non-invasive optoacoustic imaging. We have previously investigated a variety of photosensitizers acting as PA imaging contrast agents with zinc phthalocyanine emerging as the best PA contrast agent candidate [14]. Photosensitizers are attractive PA contrast agents as they are used clinically and only exert its cytotoxic effect in the presence of light in their appropriate wavelengths. While the photosensitizers can be exposed to light during PA imaging, the light energy utilized to acquire PA are not sufficient to induce singlet oxygen generation, making the photosensitizers non-toxic locally or systemically during PA imaging. Phthalocyanines constitute second-generation porphyrin-derived photosensitizers and can exist unsubstituted or with metal ions such as zinc or aluminum in its molecule, the latter of which exhibits longer triplet lifetimes and quantum yields [15, 16]. They have been shown to accumulate in tumors and exhibit a high anti-tumor efficacy in animal models and clinically with few side effects [17–19]. Nonetheless, zinc phthalocyanine being lipophilic tends to aggregate under physiological conditions [20]. In this study, we exploited Multispectral Optoacoustic Tomography (MSOT) [21, 22] as a non-invasive *in vivo* optoacoustic imaging modality to evaluate the use of water-soluble tetrasulfonated forms of phthalocyanine photosensitizers as exogenous PA contrast agents. The PA capabilities of phthalocyanine tetrasulfonic acid (PcS4), Zn(II) phthalocyanine tetrasulfonic acid (ZnPcS4) and Al(III) phthalocyanine chloride tetrasulfonic acid (AlPcS4) in a scattering phantom were evaluated. The biodistribution of the phthalocyanine photosensitizers were then tomographically visualized in an oral squamous cell carcinoma (OSCC) tumor-bearing mouse model *via* MSOT after tail vein injection.

2. Materials and methods

2.1 Absorbance measurements

Absorption spectrums of PcS4, ZnPcS4 and AlPcS4 (Frontier Scientific, U.S.A.) aqueous solutions were measured using a spectrophotometer (DU 730, Beckman Coulter) with the spectrum utilized for post-processing un-mixing of photoacoustic signals.

#224155 - $15.00 USD Received 30 Sep 2014; revised 3 Dec 2014; accepted 3 Dec 2014; published 26 Jan 2015

2.2 In vitro fluorescence imaging

Fluorescence images of aqueous solutions of PcS4, ZnPcS4 and AlPcS4 (15 μM) in microfuge tubes were taken using Xenogen IVIS Spectrum (Perkin Elmer, U.S.A.) with 640 nm as excitation and 680 nm as emission wavelengths.

2.3 In vitro and in vivo MSOT imaging system

Phantom and *in vivo* mouse photoacoustic imaging experiments were accomplished using an inVision 128 (iThera Medical GmbH, Munich, Germany) MSOT system that has been described previously [14]. An adjustable optical parametric oscillator pumped by an Nd:YAG laser provides excitation in the NIR wavelength ranging from 680 to 980 nm with a pulse span of 10 ns and repetition frequency of 10 Hz. Light from a fiber bundle divided into 10 output arms serves to illuminate the sample from multiple angles around the imaging plane. A 128-element concave transducer array spanning a circular arc of 270° was employed to detect PA signals with a central frequency of 5 MHz. The transducer array and fiber bundle outputs are submerged in a water bath maintained at 34 °C. During image acquisition, the phantom or mouse was moved through the transducer array along its axis across the volume region of interest (ROI) to capture the corresponding transverse image slices.

The PA signals of the phthalocyanine photosensitizers in phantoms were acquired utilizing cylindrical polyurethane phantoms (2 cm diameter), specifically to simulate the shape, size and optical properties of the mouse previously described in [14]. The phantom consisted of 2 inner cylindrical channels (3 mm inner diameter) to hold the photosensitizer and control samples separately (180 μL). Imaging was performed on a region of multiple transverse slices with a step size of 0.5 mm across the phantom containing the probe and control samples using 10 averages per illumination wavelength, from 680 to 900 nm in steps of 10 nm.

The animal protocols were approved by the Institutional Animal Care and Use Committee (IACUC), Biological Resource Centre, Agency for Science, Technology and Research (A*STAR), Singapore. Female NCr nude mice were injected subcutaneously with 5×10^6 OSCC cells mixed with Matrigel (BD Biosciences, San Diego, CA, USA) (1:1) each. Two weeks post-inoculation, the mice were treated with PcS4, ZnPcS4 or AlPcS4 photosensitizers (200 μL, 30 μM, ~0.25 mg/kg) *via* tail-vein injection. Ultrasound gel was applied on the mice skin surface, placed in a horizontal position in a holder under isoflurane anesthesia and wrapped in a thin polyethylene membrane to prevent contact with the water while still granting acoustic coupling. For data acquisition, a ROI of multiple transverse slices was set up with a step size of 0.3 mm from the liver to the lower abdomen region, and the averaged PA signals from 10 frames for each wavelength and position were recorded. Multispectral imaging was performed prior to injection, and various time-points post-injection. For quantitative calculation, ROIs were drawn over tumor and other organs using the transverse PA slices, with the averaged PA signals measured *via* machine integrated ViewMSOT software. The tumor PA signal was calculated from the ROI drawn around the delineation of the tumor on the slices whereby the tumor xenograft were present. The muscle PA signal was acquired from the ROI drawn in the muscle near the spinal cord to prevent interference from other internal organs' PA signals. The tumor and muscle PA signals acquired at each time point were subtracted with their respective signals acquired at pre-injection of contrast agents. A ratio of the subtracted tumor to the subtracted muscle PA signals gave the tumor/muscle PA ratio.

2.4 Image reconstruction and spectral unmixing

Images were reconstructed using a model-based method for offline analysis *via* ViewMSOT software [23]. After image reconstruction, linear spectral unmixing was employed to distinguish and isolate signals from both endogenous and exogenous chromophores [24, 25]. Maximum intensity projection (MIP) images of the photosensitizer were presented to show

#224155 - $15.00 USD Received 30 Sep 2014; revised 3 Dec 2014; accepted 3 Dec 2014; published 26 Jan 2015

relevant internal organs from different transverse slices in one 2D plane. In the MIP image of the various transverse slices acquired, the delineation of the tumor seen on individual transverse slice can be translated to the MIP image.

3. Results and discussion

PA signals of the phthalocyanines were evaluated from aqueous photosensitizer solutions (1-10 μM) and Milli-Q water as a blank control in a tissue-mimicking phantom. The wavelength range of 680 – 900 nm in 10 nm steps was chosen for phantom PA imaging due to lower tissue absorption in the near-infrared region while water absorption becomes significant above 900 nm. Upon image reconstruction, the phthalocyanines exhibited PA activity in a similar trend in waveform to that of its absorbance (Fig. 1(a)-1(c)). The correlation between absorbance and PA signal as a function of wavelength corroborated our observances as PA signals are projected from the absorbed optical energy, which is derived from the multiplication of the optical absorption coefficient and the light fluence [26]. The minor discrepancies between PA intensity and absorbance can be explained by the changes in light fluence from minor variations in laser intensity during PA imaging. The PA signals were then spectrally unmixed *via* linear regression to isolate the PA signals conferred from the photosensitizers of choice and were plotted against phthalocyanine concentration in a fitted first-order line with intercept through zero. From Fig. 1(d), PA signals of the three photosensitizers increased with their concentrations due to higher optical absorbance in observance of the Beer-Lambert law. The PcS4 line particularly exhibited the highest gradient which was approximately 1.4 and 9.3 times higher than that of ZnPcS4 and AlPcS4 lines respectively, indicating PcS4 exhibited the highest PA efficiency with concentration change followed by ZnPcS4 and more distantly by AlPcS4. This was validated from the *in vitro* fluorescence IVIS imaging of the aqueous solutions of the photosensitizers whereby AlPcS4 displayed strong fluorescence intensity at least 100 times more than that of PcS4 and ZnPcS4 upon excitation at 640 nm (Fig. 1(e)-1(f)). The poor fluorescence of PcS4 and ZnPcS4 indicated that upon excitation of their ground state molecules with response to light absorption, the excitons return to the ground state through non-radiative decay or thermally through internal conversion instead of *via* fluorescence which is a factor in remitting strong PA signals [27, 28]. ZnPcS4 is expected to be less fluorescent than AlPcS4 due to the heavy atom effect of favoring intersystem crossing rather than fluorescence [29].

We injected solutions of PcS4, AlPcS4 and ZnPcS4 intravenously in mice bearing OSCC xenograft and monitored their real-time distribution in the biological tissues using non-invasive PA imaging. In particular, the dose of the phthalocyanine photosensitizers used in this study constituted 0.25% of the observed minimum toxic dose in mice [30], ensuring no toxicity to them. MIPs based on the transverse slices scanned of the lower abdominal region were then constructed. The PA signals of the endogenous oxygenated and deoxygenated hemoglobin in one representative mouse prior to injection were shown in Fig. 2(a). The endogenous contrast agents revealed the different internal organs; mainly the kidneys, liver, spleen and intestines. The deoxygenated hemoglobin is higher in the peripheral area of the mouse possibly due to the presence of numerous superficial veins under the skin of the abdomen area (thoracoepigastric veins) that carry deoxygenated blood back to the heart as opposed to the few superficial epigastric arteries carrying oxygenated blood in the same abdomen area [31, 32]. Upon injection of PcS4, strong PA signals were detected in the liver, spleen, intestines and tumor site within the first hour post-injection of the photosensitizer, giving a good contrast between the different organs (Fig. 2(b)). After 1 h post-injection, PcS4 PA signals were seen in the kidneys, spleen and intestines to a less extent up to 24 h post-administration although contrast between the different organs was still present. ZnPcS4 on the other hand exhibited comparably less PA signal contrast between the different reticuloendothelial organs (Fig. 2(c)) as ZnPcS4 was observed to be less PA active in phantom (Fig. 1(d)). Within an hour of ZnPcS4 administration, ZnPcS4 signals could only be

#224155 - $15.00 USD Received 30 Sep 2014; revised 3 Dec 2014; accepted 3 Dec 2014; published 26 Jan 2015

discerned presumably in the kidneys, spleen and liver tissue. No specific ZnPcS4 signals were perceived thereafter. As expected, AlPcS4 produced PA signals at a much lower intensity and conferred no contrast between the different organs in the biological tissue (Fig. 2(d)). The signals were mainly on the edge of the mouse transverse slice with no signals in the organs and noise PA signals at in the background of the MIP images observed. In short, PcS4 gave the best contrast signals between the different reticuloendothelial organs which persisted up to 3 h post-administration, giving a good anatomical picture in the transverse slices.

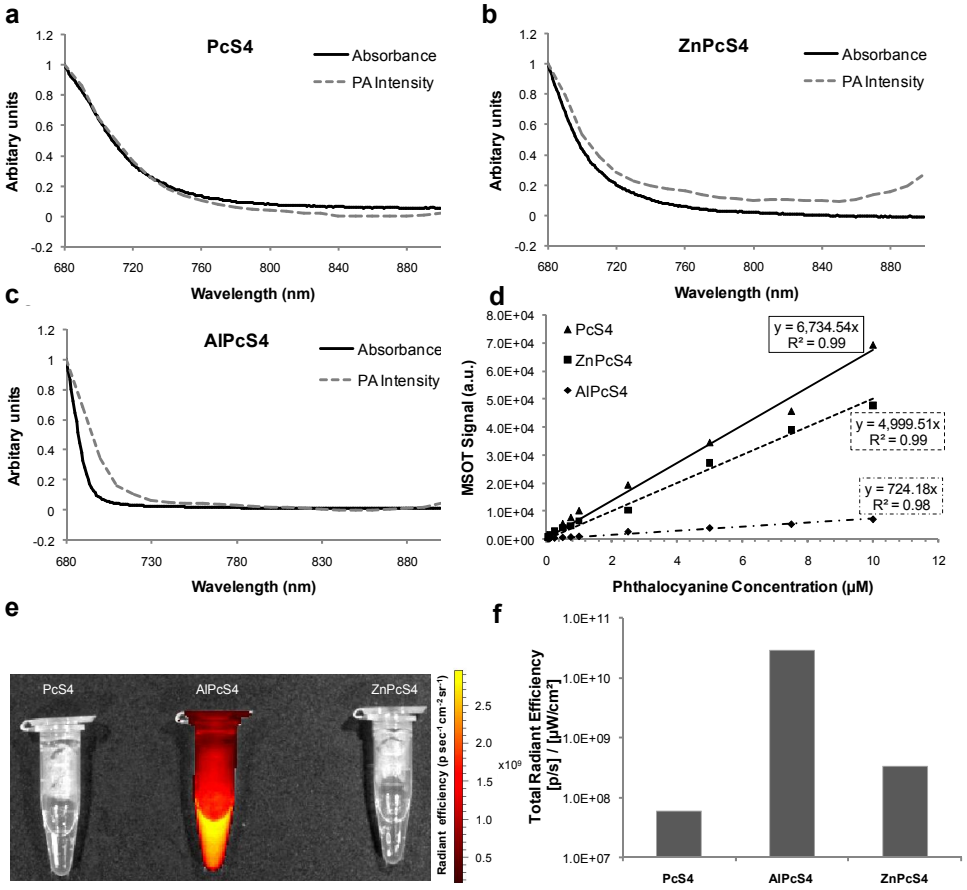

Fig. 1. Normalized absorbance and photoacoustic (PA) intensity as of values at 680 nm of (a) aluminium phthalocyanine tetrasulfonic acid (AlPcS4), (b) phthalocyanine tetrasulfonic acid (PcS4) and (c) zinc phthalocyanine tetrasulfonic acid (ZnPcS4) photosensitizers (10 μM) as a function of wavelength. A correlation between the optical absorbance and the PA ability of the photosensitizers were shown due to the similar shapes of the two graphs. (d) Multispectrally unmixed PA signals generated from AlPcS4, PcS4, ZnPcS4forms a linear relationship with phthalocyanine concentration *via* least-squares regression. (e) *In vitro* fluorescence imaging of aqueous solutions of AlPcS4, PcS4, ZnPcS4 (15 μM) with excitation at 640 nm and emission at 680 nm. (f) Quantification of radiant efficiency around region of interest in photosensitizer solutions.

#224155 - $15.00 USD Received 30 Sep 2014; revised 3 Dec 2014; accepted 3 Dec 2014; published 26 Jan 2015

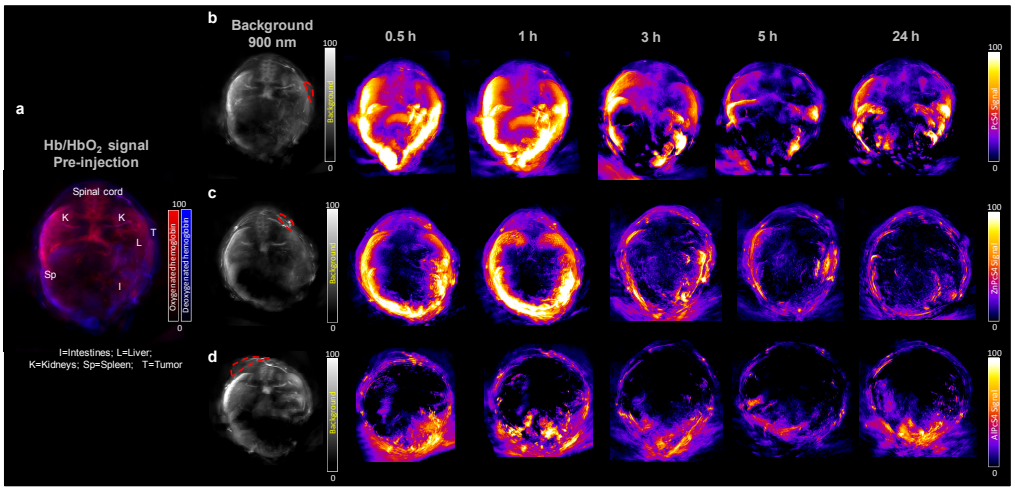

Fig. 2. In vivo MIP images showing tranverse slices of mice with OSCC xenograft tumor. (a) Oxygenated hemoglobin (HbO_2) and deoxygenated hemoglobin (Hb) signals were acquired before injection of PcS4, showing the endogenous contrast between the different organs. The red signals represent oxygenated hemoglobin while the blue signals represent deoxygenated hemoglobin in the color bar which is normalized within individual deoxygenated and oxygenated hemoglobin signals to give 0 - 100% scale. *P*hthalocyanine PA signals at various time points after tail-vein administration of (b) PcS4, (c) ZnPcS4 and (d) AlPcS4. Background PA signals from the tissues were acquired at 900 nm laser wavelength with the dashed red lines delineating tumor tissue.

The PA signals of the phthalocyanines can also be semi-quantified *via* MSOT to reveal their biodistribution and their clearance pathways. PcS4 signals gave considerable tomographic contrast between the different organs within an hour post-administration with signals strongest in the spleen, intestines and liver (Fig. 2(b)). This was confirmed through quantitative analysis whereby high concentrations of PcS4 signals were found in intestines, liver and spleen at 30 mins post-administration which gradually dropped with time (Fig. 3(a)). The high signals in intestines and spleen suggested that the PcS4 was primarily eliminated *via* bile-gut elimination pathway. The considerable signals in the kidneys also insinuated that the photosensitizer was secondarily eliminated through renal pathway. PcS4 signals in the OSCC tumor were observed to be at its peak at 1 h post-administration after which the signal decreased over time (Fig. 2(b)). It is known that increasing the number of sulfonate groups in phthalocyanine facilitate tumor localization [33]. Although nanoparticle-based contrast agents can accumulate in tumors effectively by passive or active targeting, small molecule-based contrast agents are attractive as they do not involve uniformity control and preparation techniques. From Fig. 3(b), ZnPcS4 signals were about 3 times lower in intensity than that of PcS4 in the various organs and tissues. Similarly, ZnPcS4 signals were the highest in the intestines, liver and spleen regions while intensity in tumor remains comparable at all time points. AlPcS4 signals on the other hand were about 500 times less intense than that of PcS4 and appeared comparable in all tissues at all time points, indicating no signal contrast between the different internal organs (Fig. 3(c)). Tumor/muscle ratio of the PA signals from PcS4 revealed a peak value at 1 hour, indicating this may be an ideal time point for photodynamic therapy illumination (Fig. 3(d)). Tumor/muscle ratio of the PA signals from both ZnPcS4 and AlPcS4 were comparable between the different time points with tumor/muscle ratio of PcS4 signal at 1 h post-injection significantly higher than that of ZnPcS4 and AlPcS4 ($p < 0.05$). In all, PcS4 emerged as the best PA contrast agent among the tetrasulfonate phthalocyanines studied. As PcS4 accumulated in the tumor with a peak value at 1 h post-injection, this suggests to us the ideal time for photodynamic therapy or photodiagnostics. Due to its accumulation in the tumor, it offers a theranostic approach when combined with

#224155 - $15.00 USD Received 30 Sep 2014; revised 3 Dec 2014; accepted 3 Dec 2014; published 26 Jan 2015

photodynamic therapy whereby PA visualization and anti-tumor therapy could be achieved concurrently. The light utilized in the MSOT can be tuned to induce photodynamic therapy, making combined imaging and therapy a future endeavor that we can investigate. Additionally, non-invasive PA imaging was successfully utilized to image small molecule contrast agents tomographically.

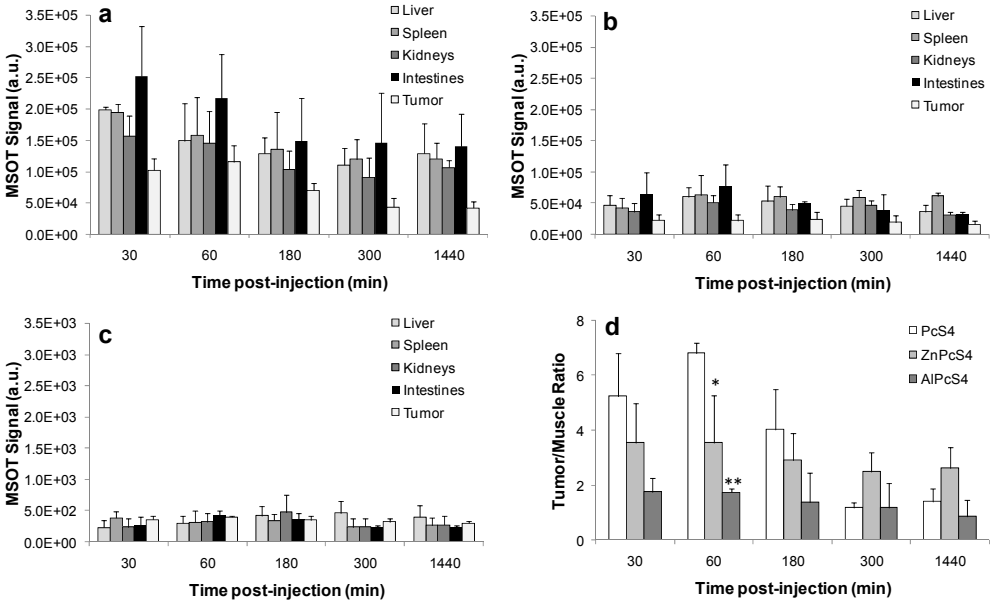

Fig. 3. Biodistribution of (a) PcS4, (b) ZnPcS4 and (c) AlPcS4 in various tissues and (d) tumor/muscle ratios of PA signals for the different phthalocyanine photosensitizers at different time points post-administration (mean ± SD, $n = 3$, Student's t-test, $*p < 0.05$, $**p < 0.005$).

4. Conclusions

Three types of tetrasulfonate phthalocyanines (PcS4, ZnPcS4 and AlPcS4) were studied herein for their PA activity and their potential as PA contrast agents. The PA activity of these photosensitizers were studied in phantom showing that PcS4 and ZnPcS4 exhibited strong PA capabilities while AlPcS4 displayed the lowest change in PA signal with concentration increase. Thereafter, we successfully imaged and semi-quantified the biodistribution of phthalocyanine photosensitizers using tomographic and non-invasive PA imaging of tumor-bearing mice. Upon administration of the phthalocyanines in mice bearing OSCC tumor xenograft, PcS4 exhibited the strongest PA signal while displaying good contrast between the organs in the lower abdominal region, giving anatomical information and also biodistribution of the photosensitizer. Since PcS4 gave the highest PA activity in phantom compared to the other phthalocyanines, it conferred good PA signals upon administration in OSCC-bearing mice. PcS4 PA signals were seen in the kidneys, liver, spleen, intestines and tumor sites within an hour after injection. ZnPcS4 signals did not confer much contrast given to other organs. AlPcS4 merely produced noise signals due to its minimal PA activity as studied in phantom. PcS4 accumulated in the tumor with a peak value at 1 h post-injection, suggesting this is the ideal time for photodynamic therapy or photodiagnostics. PcS4 has proved itself to be a useful contrast agent in an alternative imaging technique.

Acknowledgments

This work was supported by the Singapore Bioimaging Consortium, Agency for Science, Technology and Research, Singapore.